

# Localized random projections with applications to coherent array imaging

Rakshith Sharma Srinivasa, Mark A Davenport, Justin Romberg  
Georgia Institute of Technology

**Abstract**—We consider the standard active array imaging problem and propose a novel trade-off that enables the imaging of range limited target scenes with far fewer measurements than conventional techniques by exploiting the bandwidth of the known excitation signal. Unlike standard compressed sensing, we do not assume that the scene is sparse, only that it is range limited. We abstract the proposed method as a novel matrix sketching problem that utilizes a few localized random projections in the row space of a matrix to capture the full row space. We provide mathematical guarantees on the number of such projections required. We present imaging simulation results that support our theoretical results.

## I. INTRODUCTION

**S**TANDARD coherent array imaging illuminates targets with a known waveform and images them by measuring the reflections. The angular resolution of the reconstructed image is a function of the aperture size and the number of antenna elements used in the array. To form a reconstruction at the highest resolution, a number of measurements equal to the number of array elements is required. However, the task of reading out measurements from large densely sampled arrays is challenging.

In this paper, we propose a novel trade-off that utilizes excitation bandwidth to image range limited target scenes with far fewer measurements compared to conventional imaging techniques. This can have an impact on both the cost of operating the array as well as acquisition times. The decrease in the number of measurements is a result of the reduced number of degrees of freedom that range limited images induce on broadband measurements.

We show that the proposed trade-off can be abstracted as a novel matrix sketching problem: capturing the range space of a linear operator using only *localized* random projections of the range space. Localized random projections are used in many scenarios such as streaming, online, multimodal, and distributed data acquisition where one can only partly access data at a given instant. In particular, we consider a *repeated block diagonal*

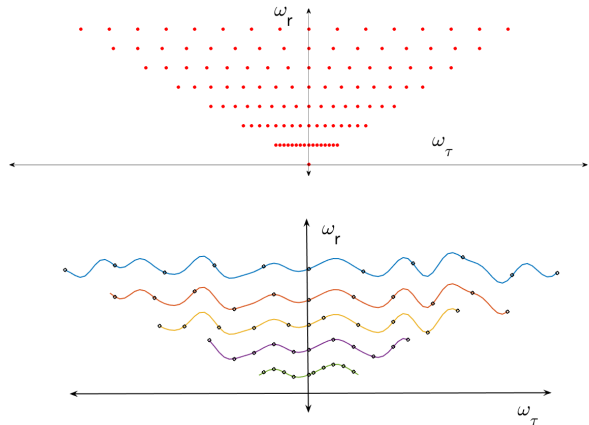


Fig. 1: Array measurements as samples on a pseudopolar grid in the Fourier domain (top). For an image at a constant range, the array measurements at different frequencies are samples of a common function (bottom)

matrix and provide conditions on the linear operator that render this structured sketching matrix as effective as a general unstructured sketching matrix.

Our model focuses on far-field antenna array imaging. Antenna array measurements of far-field targets (magnitude and phase) are direct samples of the Fourier domain of the target scene. Figure 1 (top) shows the area in the Fourier domain that is sampled as a result of signal acquisition in the case of a 1D array. For general range limited scenes, the functions sampled at different frequencies (Figure 1 (bottom)) have a limited number of degrees of freedom. In the extreme case of a scene with delta thickness (only one reflector per angle), the functions sampled at different frequencies are the same. For such a scene, when a full read-out is performed at the frequency the array is designed for (inter-element spacing of  $c/2f$  where  $c$  is the speed of light), measurements at lower frequencies offer redundant information. For general range-limited scenes, the number of degrees of freedom of the ensemble of samples at lower frequencies is limited. In general, the number of degrees of freedom

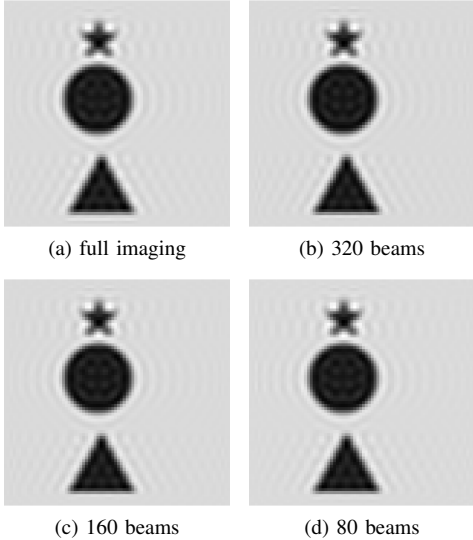


Fig. 2: Aperture coded imaging for images at a constant range. (a) represents the conventional method, which uses about 1100 beams

decreases as the range limit decreases (see Figure 1 (bottom) ). This redundancy can be used to spatially subsample the array while using broadband excitation.

Figure 2 provides an illustration of the effectiveness of the proposed scheme. A target scene at a constant known depth that typically requires about 1100 measurements/beams when imaged using narrowband excitation can be imaged with only roughly 80 beams with no loss in resolution, when broadband excitation is used. The setup used for this simulation is described in Section V.

We provide the following theoretical results: (i) a lower bound on the number of measurements needed for a given excitation bandwidth (Theorem 1) and (ii) conditions on a set of  $k$  excitation frequencies that can result in fewer measurements by a factor of  $k$ . We then provide simulation results for some imaging experiments that support our proposed trade-off and theoretical analysis.

This paper is organized as follows. In Section II, we review the available literature on the two main relevant areas: coherent imaging and matrix sketching. In Section III, we develop the model for our proposed array signal acquisition method. In Section IV, we provide signal recovery guarantees for the proposed method. The theoretical results are also of general interest in the matrix sketching field. In Section V, we provide simulation results for various imaging experiments.

## II. RELATED WORK

In this section, we review the work most related to this paper. Our work is targeted towards efficient array processing and uses techniques from numerical linear algebra to provide recovery guarantees. We provide references to both of these fields below.

### A. Array imaging

Standard array imaging problems have been considered in [1], [2] where the inverse problem is set up using transmit and receive *beamforming* with narrowband excitation. General 3D imaging with wide-band excitation is considered in [3]. In general, to identify a 3D scene, a 2D antenna array and broadband excitation are necessary. We identify the limited number of degrees of freedom in a range limited image and show that such a scene can be captured using far fewer measurements compared to conventional methods. Efficient array processing has been an active area of research, in order to reduce the operating costs of antenna arrays. By using a carefully designed non-uniform array, [4] proposes to increase the number of resolvable directions to  $O(N^2)$  by using an array with  $O(N)$  elements. Another main theme in reducing the cost of array systems has been the use of compressed sensing techniques. Reducing sampling rates at the sensors for digital beamforming is proposed in [5]–[7], but the number of beams/ array elements remain the same as conventional imaging. Sparsity based regularization is imposed in [8] to solve the ill-posed radio-interferometric imaging problem. A similar theme is also followed in [9] which addresses the problem of 3D imaging with a 2D phased array, but assumes sparsity in the image domain. We do not assume any sparsity in the image domain and directly address the number of measurements/beams required to obtain the best possible reconstruction.

Array imaging of range limited images is a particular example of an application that concerns simultaneous concentration of a signal in temporal/spatial domain and frequency domain. Analysis of the number of degrees of freedom of such signals was performed in [10]–[13] and [14], [15]. Our observation of the reduced number of degrees of freedom in the context of array imaging stems from these papers.

### B. Matrix sketching

We show that our proposed method can be modeled as a novel matrix sketching problem. Matrix sketching refers to a set of techniques in numerical linear algebra for dimensionality reduction. In particular, a given large matrix is pre/post multiplied by a suitable matrix to

reduce the ambient dimensions while still approximately preserving important information. Research in this area has seen a rise in popularity due to its utility in the big data setting [16], [17]. Our theoretical results are more aligned with those in [18] where random Gaussian projections are used to capture the range space of linear operators. In the context of imaging, usage of sketching ideas can be seen in [19] where the Fourier basis is used as a sketching matrix for dimensionality reduction in interferometry but the sketching matrix in their setup is a generic rectangular sketching matrix. In our proposed model, the sketching matrix involved itself has a very particular structure that is dictated by the physical antenna array setup, which introduces new challenges.

### III. SIGNAL MODEL

#### A. Array imaging setup

In this section, we describe the standard linear model for far-field imaging. We present here the model for a 1D array, which can be easily extended to 2D arrays.

Consider a uniform linear array of aperture length  $D$  consisting of  $M$  elements placed on the X-axis at locations  $-d_{M/2} \dots, d_{M/2} \in [-D/2, D/2]$ . The scene to be imaged lies in the X-Y plane and in the far-field region of the array. Let the reflectivity map, a function of the round-trip distance of the target from the array center and the angle from the broadside, be denoted as  $p(r, \theta)$ . The system consists of only one transmitting element which is co-located with the receiver at the array center. This system can hence be classified as single-input multiple-output (SIMO). For an excitation signal  $s(t)$ , the output of the  $m^{\text{th}}$  element is  $s(t - r_0/c - d_m \sin \theta_0/c)$ , for a unit-strength reflector at  $(r_0, \theta_0)$ . For a general reflectivity map within a range limit  $R$ , the narrowband response for an excitation signal  $e^{j2\pi ft}$  is

$$y_m(t) = e^{j2\pi ft} \int_{-\pi/2}^{\pi/2} \int_{-R}^R p(r, \theta) e^{-j2\pi(r + d_m \sin \theta)/\lambda} dr d\theta. \quad (1)$$

The reflectivity map can be deduced using the wavelength dependent amplitude of the received signal. By letting  $\tau = (\sin \theta)/2$ , the output of  $m^{\text{th}}$  element at excitation wavelength  $\lambda$  can be written as

$$y_m(\lambda) = \hat{x}_c(\omega_r, \omega_\tau), \quad \omega_r = \frac{1}{\lambda}, \quad \omega_\tau = \frac{2d_m}{\lambda} \quad (2)$$

where  $\hat{x}_c$  is the Fourier transform of  $x_c(r, \tau)$ ,  $x_c(r, \tau) = \frac{p(r, \sin^{-1}(2\tau))}{\sqrt{1-4\tau^2}}$  in the continuous domain.

For computational purposes, we discretize the scene as vector of uniformly placed points. The ensemble

of measurements collected at different frequencies is shown in Figure 1 (top). The antenna imaging system at excitation frequency  $f$  can be modeled as  $y_f = A_f x_0$  where  $x_0$  is the scene reflectivity at the sampled points,  $A_f$  is the matrix mapping the scene to the array outputs and  $y_f$  is the vector of array outputs.  $A_f \in \mathbb{C}^{M \times N}$  where  $N$  is the number of spatial samples and  $M$  is the number of array elements. With multiple excitation frequencies, array measurements of length  $M$  are obtained at each frequency. Let the array output at frequency  $f_i$  be  $y_{f_i}$  and the corresponding matrix operator be  $A_{f_i}$ . Letting  $y = [y_{f_1}^T \ y_{f_2}^T \ \dots \ y_{f_k}^T]^T$  and  $A = [A_{f_1}^T \ A_{f_2}^T \ \dots \ A_{f_k}^T]^T$ , the imaging system with multiple frequencies can be modeled as

$$y = Ax_0. \quad (3)$$

#### B. Proposed measurement model

The array outputs can be acquired in a variety of ways. One way is to perform a direct read-out of the array as (3) shows. Another standard approach is to obtain specific linear combinations of the array outputs. When the linear combinations induce spatial directivity, the procedure is termed *beamforming* and the antenna array *scans* over the scene. This can be modeled as

$$z_{f_i} = \psi y_{f_i} = \psi A_{f_i} x_0 \quad (4)$$

where  $\psi$  is an  $M \times M$  matrix with each row representing one set of weights.

Both the above schemes obtain  $M$  measurements to obtain the best possible resolution: either  $M$  direct read-outs from the antenna array or  $M$  *beams* in beamforming.

Our proposed method is to obtain fewer *generic* linear combinations or *coded aperture measurements* at multiple frequencies. Let  $\phi \in \mathbb{R}^{l \times M}$  matrix where each of the  $l$  rows represent a set of weights used to form a linear combination of the array outputs. Each linear combination corresponds to one *generic beam*. The sampled value is a linear combination of the element outputs just as in spatial beamforming. A single set of weights can be used to obtain measurements at all excitation frequencies by using broadband excitation and taking a temporal Fourier transform. However, this imposes that the same set of aperture codes be used at all frequencies. One measurement would correspond to obtaining a linear combination with a *fixed* set of weights of each row of points in Figure 1 (top). This results in the following model:

$$\Phi y = \Phi A x_0 = Y x_0, \quad (5)$$

where  $\Phi$  is a block diagonal matrix with  $k$  repeated blocks, as shown below

$$\Phi = \begin{bmatrix} \phi & 0 & \cdots & 0 \\ 0 & \phi & \cdots & 0 \\ 0 & 0 & \cdots & \phi \end{bmatrix}. \quad (6)$$

We refer to such a matrix as a repeated block diagonal (RBD) matrix. Even though we obtain compressive measurements, unlike standard compressed sensing regimes, we do not assume any sparsity in the target scene. Integrating further structure in the target scene will of course result in better sample complexity. But our intention is to study just the range limited model. We will use the ordinary least squares reconstruction

$$\arg \min_x \|y - Ax\|_2^2. \quad (7)$$

With aperture coding in place, this becomes

$$\arg \min_x \|\Phi y - \Phi Ax\|_2^2. \quad (8)$$

Our goal is to show that the solutions of (7) and (8) are equal for range limited images, for  $l < M$ .

#### IV. SIGNAL RECOVERY GUARANTEES

In this section, we consider the general problem (8) and derive bounds on the number of random projections in each diagonal block  $l$  required to faithfully solve it. Let  $r_i$  denote the rank of  $A_i$ . If  $l \geq \max_i r_i$ , it is straightforward to see that the solutions of (7) and (8) match. We are interested in sharper bounds for  $l$ . In general, if  $\Phi$  is such that the rowspaces  $\text{row}(\Phi A)$  and  $\text{row}(A)$  are the same, then (7) and (8) have the same solution. A necessary and sufficient condition is for the rowspaces to be equal is:

$$\|(I - P_{A^* \Phi^* A^*})\| = 0, \quad (9)$$

where  $P_M$  denotes the orthogonal projection onto the column space of range of  $M$ .

Repeated block diagonal matrices can provide only *local* random projections of the row space of  $A$ . Our main insight is that when row spaces of  $A_i$ 's are not orthogonal, localized random projections in the row space of  $A_i$  provide information about the row spaces of  $A_j$ ,  $j \neq i$  as well. This translates to a lack of degrees of freedom in the ensemble of points in Figure 1 (top). Linear combinations of a row of points in this ensemble provide information about the samples in other rows as well (corresponding to different frequencies).

We present two main results in this section: (i) A simple, but non-trivial lower bound on  $l$  for which (9) holds, and (ii) A sufficient condition on a given ensemble  $\{A_i\}$ ,  $i = 1, \dots, k$  for which  $l \geq \lceil r/k \rceil$  suffices for (9)

to hold, where  $r$  is the rank of  $A$ . Note that  $\lceil r/k \rceil$  is a fundamental lower bound on  $l$ .

To establish the first result, we factorize the linear operator to reveal the dependence between the row spaces of  $A_i$ :

$$A = \begin{bmatrix} A_1 \\ A_2 \\ \vdots \\ A_k \end{bmatrix} = \begin{bmatrix} C_{11} & 0 & \cdots & 0 \\ C_{21} & C_{22} & \cdots & 0 \\ \vdots & \vdots & \cdots & \vdots \\ C_{k1} & C_{k2} & \cdots & C_{kk} \end{bmatrix} \begin{bmatrix} V_1^T \\ V_2^T \\ \vdots \\ V_k^T \end{bmatrix} = CV^T, \quad (10)$$

where  $C_{ij} \in \mathbb{R}^{m \times d_j}$  and each  $C_{ii}$  is full column rank when  $d_i \neq 0$ ,  $V$  is an  $r \times n$  orthonormal matrix. The factorization is such that the row space of  $A_1$  is the span of the orthobasis  $V_1$ , the row space of  $A_2$  is included in the span of  $V_1$  and  $V_2$ . In general,  $[V_1 \ V_2 \ \cdots \ V_k]$  includes an orthobasis for the row space of  $A_i$ . This factorization is equivalent to a block QR factorization of  $A^T$  and can be obtained for any general matrix  $A$ . Each  $d_i$  represents the innovation that a new group  $A_i$  adds to the row space of the already existing ensemble  $\{A_i\}$ ,  $j < i$ . Note that  $\sum_i d_i = \text{rank}(A)$ . Our first result states that if  $l \geq \max_i d_i$ , then (9) holds true.

*Theorem 1:* For a given matrix  $A$  of size  $km \times n$ , let  $d_i$ 's be defined as in (10) and let  $p$  be a small oversampling factor. Let  $\Phi$  be a block diagonal matrix with repeated diagonal block  $\phi$  of size  $l \times m$  and whose entries are chosen i.i.d. from the standard normal distribution. Let  $Y = \Phi A$ . Define  $d_0 = \max_i d_i$ . For

$$l \geq d_0 + p \quad (11)$$

$\|(I - P_{Y^*})A^*\| = 0$  with probability 1.

Theorem 1 shows that a number of random projections greater than the *innovation* that each new operator  $A_i$  offers suffices to capture the union of subspaces of all  $A_i$ 's. In other words, a given set of localized random projections  $\phi A_i$  need not capture the entire row space of any  $A_i$ . If the subspaces  $\text{row}(A_i)$  overlap, a linearly independent set of vectors that capture the row space of the whole matrix can be obtained by using a few random projections of each row group. The factorization in (10) captures this dependence between the subspaces spanned by the row groups.

This result is particularly useful when  $\text{row}(A_i) \subset \text{row}(A_j) \ \forall i < j$ . If the overlap between the subspaces is not considered,  $l \geq \max_i \text{rank}(A_i) = \sum_i d_i$  random projections per block would be necessary. However, as seen from 1, fewer projections may be sufficient. On the other hand, when the row spaces are all mutually orthogonal, then Theorem 1 clarifies that  $l \geq \max_i \text{rank}(A_i)$  is necessary.

In the context of array imaging and a scene at a known constant depth, the ensemble  $\{A_i\}$  has the favorable

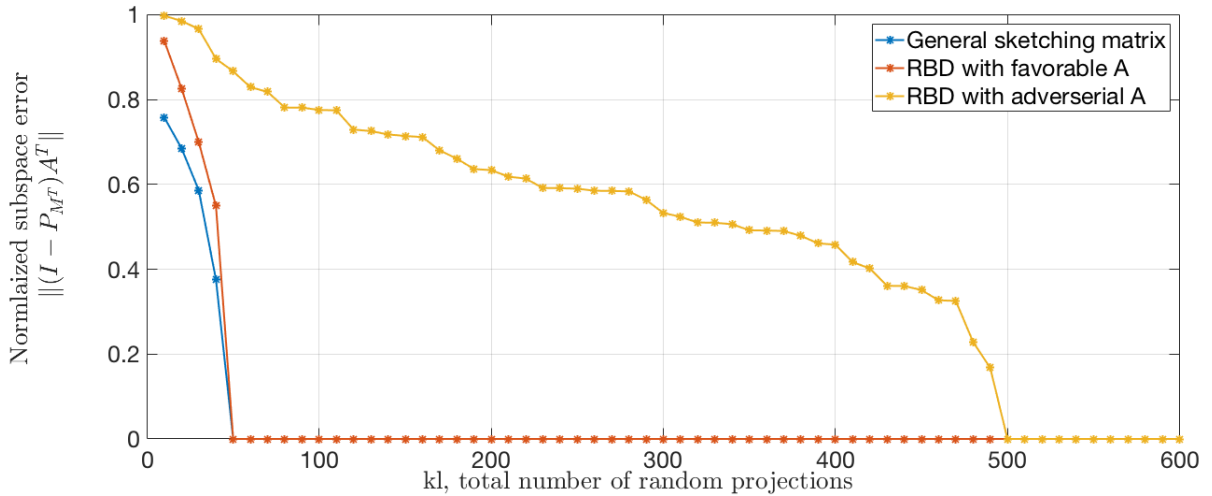


Fig. 3: Comparison of the sample complexity  $l$  required to capture the row space using a generic sketching matrix and a RBD sketching matrix. The entries of the sketching matrices are all drawn from the standard Gaussian distribution. While using an RBD matrix for sketching, the favorable case realization of  $A$  obeys the condition required by Theorem 2 while the adversarial case realization of  $A$  does not.

nested subspace structure with the corresponding  $d_i$ 's being equal to  $2A(f_i - f_{i-1})/c$  where  $f_i, f_{i-1}$  are consecutive excitation frequencies,  $A$  is the aperture size. Similarly,  $d_1 = 2Af_{\min}/c$  where  $f_{\min}$  is the smallest excitation frequency used. If consecutive frequencies are placed close enough, a simple estimate of the number of aperture codes required is proportional to  $f_{\min}$ . This is lower than that of conventional imaging, where the number of beams used is proportional to  $f_{\max}$ .

Although the estimate provided by Theorem 1 improves over conventional imaging techniques, dependence on the smallest frequency can be further improved. We now present our second main result. Suppose that  $\Phi$  was a general sketching matrix and  $\text{rank}(A) = r$ . Then, a total number of random projections greater than  $r$  would suffice for (9) to hold. It is then natural to ask if  $kl \geq r$  suffices when  $\Phi$  is an RBD sketching matrix. We answer this question in the following theorem. For the sake of convenience, we assume that  $r = nk$  for some integer  $n$ , but the result holds in general, with the condition  $l \geq r/k$  replaced by  $l \geq \lceil r/k \rceil$ .

**Theorem 2:** Given an ensemble of  $k$  matrices  $\{A_i\}$  each of size  $m \times n$  and a matrix  $\phi \in \mathbb{R}^{l \times m}$  with entries drawn from the standard normal distribution,  $M = [(\phi A_1)^T \ (\phi A_2)^T \ \cdots \ (\phi A_k)^T]^T$  is full row rank if there exists an orthobasis  $V$  in  $\mathbb{R}^m$  and an index set  $\mathcal{S}$ ,  $\mathcal{S} \subset [n]$ ,  $|\mathcal{S}| = l$  such that the  $kl \times n$  size matrix  $\hat{M} = [(V_{\mathcal{S}} A_1)^T \ (V_{\mathcal{S}} A_2)^T \ \cdots \ (V_{\mathcal{S}} A_k)^T]^T$  has full row rank. Consequently, if these conditions are met for  $l \geq r/K$ ,  $\|(I - P_{M^T})A^T\| = 0$  with probability 1.

Intuitively, since the structure of  $\Phi$  imposes the *same* set of random projections on each block, in order to obtain linearly independent random projections, the corresponding rows of  $A_i$ 's should themselves be linearly independent. If there still exists a set of corresponding rows that are linearly independent modulo a basis change, the number of random projections  $l$  required can be very low when the row spaces of  $A_i$  overlap to a high degree.

Figure 3 shows a simulation result that compares the total number of random projections needed by a generic sketching matrix to that of an RBD sketching matrix. For the simulation,  $k = 10$  was used, with  $\text{rank}(A) = 50$ . In the latter case, two different linear operators  $A$  were generated, one that obeys the conditions of Theorem 2 and one that does not. We can see from the figure that the sample complexity  $l$  does depend on the matrix  $A$ .

## V. NUMERICAL RESULTS

We test our proposed model by simulating various imaging scenarios. Array parameters used in all the simulations are: an array of  $40 \times 40$  elements, with 15 excitation frequencies placed regularly in the bandwidth of 2GHz - 4GHz. The elements were placed at half the wavelength of the highest frequency. The scene was assumed to be within the angular span of  $[-\pi/4, \pi/4]$  in both directions. For this configuration the full set of measurements would be approximately around 1100. Quantitative error values for all the experiments are given in Table I.

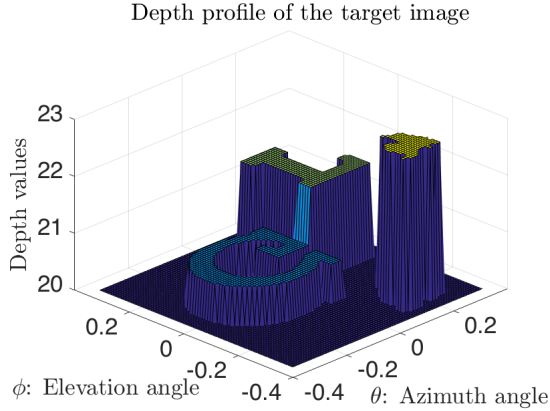


Fig. 4: Depth map of the multi-depth image used in simulations

In the first set of experiments, we consider a scene with delta thickness at a constant, known depth. Conventional beamforming requires about 1100 beams with excitation using  $f_{\max}$  (4GHz) to scan over the entire image. Image reconstruction results are shown in Figure 2. We can see that using as few as 80 beams with broadband excitation, similar reconstruction performance can be obtained. The relative reconstruction error is almost negligible in each case (shown in Table I).

Aperture coding is also effective for multi-depth images, where reflectors at different angles maybe present at different depths. A scene with three segments, each at a different depth was used in our simulations. The depth map of the scene is shown in Figure 4.

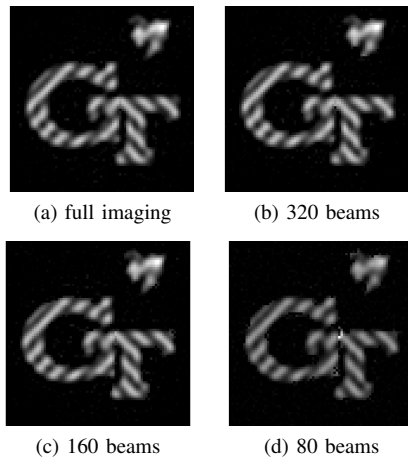


Fig. 5: Aperture coded imaging for a multi-depth image. (a) represents the conventional method, which uses about 1100 beams.

Figure 5 shows reconstruction results for the multi-depth scene considered. Again only about 80 beams are

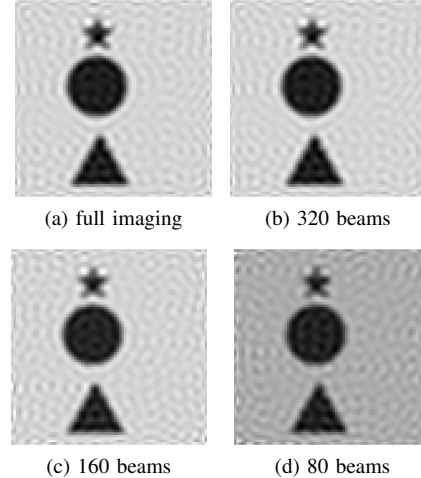


Fig. 6: Aperture coding in the presence of noise. The regularization parameters was varied in each case to match the SNR of the full imaging scenario. The noise performance was preserved without compromising on the signal reconstruction quality, as seen in table II.

sufficient to get good quality results. For such images, even though the points along different rows in Figure 1 are different, they have few degrees of freedom.

We further test our proposed acquisition scheme under noisy regimes. Figure 6 shows reconstruction results in the presence of noise with an SNR of 20dB . The corresponding signal reconstruction error values and output SNR are given in Table I. It is clear that aperture coded measurements do not result in any degradation in the presence of noise. This shows that the sketched matrix is not only full rank, but also has stable singular values.

Drawing further inspiration from techniques in numerical linear algebra, we conducted simulations with subsampled arrays instead of using codes drawn from the Gaussian distribution. Subsampling the rows/columns instead of taking random projections is a common technique of dimensionality reduction [20]. This can be thought of as aperture coding with binary codes. Reconstruction error values obtained are shown in Table II. We can see that subsampling an array is as effective as using a full array when broadband excitation is used.

These results demonstrate that range limited target scenes induce a finite number of degrees of freedom on the ensemble broadband array measurements. The array imaging operators associated with such scenes allow for a stable reconstruction from compressive or subsampled measurements without any structural assumptions on the scene such as sparsity. The proposed trade-off with excitation bandwidth can be readily implemented in existing

Imaging mode	Constant range	Flat image	Multi-depth	Constant range noisy	
				Signal error	OP SNR
Full imaging (1100 beams)	NA	NA	NA	NA	16.09
320 codes	2.7e-5	4.4e-4	3e-4	2.5e-5	16.0117
160 codes	7.4e-5	3.3e-4	1.2e-3	6.3e-5	15.9112
80 codes	4.2e-4	5.1e-4	4.8e-2	4.9e-4	15.3206

TABLE I: This table shows the relative reconstruction error values for different classes of images. Aperture codes with weights chosen from standard Gaussian distribution were used.

array imaging systems which are typically broadband and hence is an effective way of imaging range limited scenes.

Imaging mode	CR	FS	MD
320 elements	2e-4	1e-4	1e-3
160 elements	9e-4	4e-4	3.1e-2
80 elements	1.6e-3	1.1e-3	5.8e-3

TABLE II: Relative reconstruction errors with subsampled array: The array was randomly subsampled to have 320, 160 and 80 elements. CR: constant range image, FS: Flat image, MD: Multi-depth image

## REFERENCES

- [1] S. Patole and M. Torlak. Two dimensional array imaging with beam steered data. *IEEE Trans. Image Process.*, 22(12):5181–5189, 2013.
- [2] M. Soumekh. Array imaging with beam-steered data. *IEEE Trans. Image Process.*, 1(3):379–390, 1992.
- [3] D. Sheen, D. McMakin, and T. Hall. Three-dimensional millimeter-wave imaging for concealed weapon detection. *IEEE Trans. Microw. Theory and Techn.*, 49(9):1581–1592, 2001.
- [4] P. Pal and P. Vaidyanathan. Nested arrays: A novel approach to array processing with enhanced degrees of freedom. *IEEE Trans. Signal Process.*, 58(8):4167–4181, 2010.
- [5] M. Birk, A. Burshtein, T. Chernyakova, A. Eilam, J. Choe, A. Nikoozadeh, P. Khuri-Yakub, and Y. Eldar. Compressed 3d ultrasound imaging with 2d arrays. In *2014 IEEE International Conference on Acoustics, Speech and Signal Processing (ICASSP)*, pages 6919–6923, May 2014.
- [6] T. Chernyakova and Y. Eldar. Fourier-domain beamforming: the path to compressed ultrasound imaging. *IEEE Trans. Ultrason., Ferroelect., and Freq. Control*, 61(8):1252–1267, 2014.
- [7] N. Wagner, Y. Eldar, and Z. Friedman. Compressed beamforming in ultrasound imaging. *IEEE Trans. Signal Process.*, 60(9):4643–4657, 2012.
- [8] Y. Wiaux, L. Jacques, G. Puy, A. Scaife, and P. Vanderghenst. Compressed sensing imaging techniques for radio interferometry. *Monthly Notices of the Royal Astronomical Society*, 395(3):1733–1742, 2009.
- [9] Q. Cheng, A. Alomainy, and Y. Hao. Compressive millimeter-wave phased array imaging. *IEEE Access*, 4:9580–9588, 2016.
- [10] D. Slepian. On bandwidth. *Proceedings of the IEEE*, 64(3):292–300, 1976.
- [11] D. Slepian and H. Pollak. Prolate spheroidal wave functions, fourier analysis and uncertainty I. *Bell System Technical Journal*, 40(1):43–63, 1961.
- [12] H. Landau and H. Pollak. Prolate spheroidal wave functions, fourier analysis and uncertainty II. *Bell System Technical Journal*, 40(1):65–84, 1961.
- [13] H. Landau and H. Pollak. Prolate spheroidal wave functions, fourier analysis and uncertainty III: The dimension of the space of essentially time- and band-limited signals. *Bell System Technical Journal*, 41(4):1295–1336, 1962.
- [14] F.J. Simons. *Slepian Functions and Their Use in Signal Estimation and Spectral Analysis*, pages 891–923. Springer Berlin Heidelberg, Berlin, Heidelberg, 2010.
- [15] F.J. Simons and Dong V. Wang. Spatiospectral concentration in the cartesian plane. *GEM - International Journal on Geomatics*, 2(1):1–36, Jun 2011.
- [16] J. Yang, X. Meng, and M. Mahoney. Implementing randomized matrix algorithms in parallel and distributed environments. *Proceedings of the IEEE*, 104(1):58–92, 2016.
- [17] D. Woodruff. Sketching as a tool for numerical linear algebra. *Foundations and Trends in Theoretical Computer Science*, 10(12):1–157, 2014.
- [18] N. Halko, P. Martinsson, and J. Tropp. Finding structure with randomness: Probabilistic algorithms for constructing approximate matrix decompositions. *SIAM Review*, 53(2):217–288, 2011.
- [19] S.V. Kartik, R. Carrillo, J.P. Thiran, and Y. Wiaux. A fourier dimensionality reduction model for big data interferometric imaging. *Monthly Notices of the Royal Astronomical Society*, 468(2):2382–2400, 2017.
- [20] P. Ma, M. Mahoney, and B. Yu. A statistical perspective on algorithmic leveraging. In *Proceedings of the 31st International Conference on Machine Learning*, volume 32 of *Proceedings of Machine Learning Research*, pages 91–99, Beijing, China, 22–24 Jun 2014. PMLR.